Small-Molecule Modulators of Lipid Raft Stability and Protein-Raft Partitioning

Katherine M. Stefanski[1,2], Hui Huang[1,2], Dustin D. Luu[3], James M. Hutchison[4], Nilabh Saksena[1,2], Alexander J. Fisch[1,2], Thomas P. Hasaka[1,5], Joshua A. Bauer[1,5], Anne K. Kenworthy[6], Wade D. Van Horn[3], Charles R. Sanders[1,2]

Affiliations:

1. Department of Biochemistry, Vanderbilt University School of Medicine, Nashville, Tennessee, USA

2. Center for Structural Biology, Vanderbilt University School of Medicine, Nashville, Tennessee, USA

3. School of Molecular Sciences, The Virginia G. Piper Biodesign Center for Personalized Diagnostics, The Biodesign Institute, Arizona State University, Tempe, AZ, USA.

4. Department of Pharmacology, Yale University School of Medicine, New Haven, CT 06520, USA; Yale Cancer Biology Institute, Yale University West Campus, West Haven, CT, USA.

5. Vanderbilt Institute of Chemical Biology, High-Throughput Screening Facility, Vanderbilt School of Medicine, Nashville, Tennessee, USA

6. Center for Membrane and Cell Physiology and Department of Molecular Physiology and Biological Physics, University of Virginia School of Medicine, Charlottesville, VA, USA

ABSTRACT

The functions of phase-separated ordered membrane domains, colloquially known as lipid rafts, have yet to be well-defined, in part because of a lack of tools to manipulate raft formation and protein affinity for rafts. Human peripheral protein 22 (PMP22) exhibits a high affinity for lipid rafts in giant plasma membrane vesicles (GPMVs). We screened 24,000+ small molecules in search of compounds that alter the raft affinity of PMP22. Hits were counter-screened against another raft partitioning protein, MAL, and also were tested for their impact on raft formation. We describe the discovery of two classes of compounds. Class I molecules altered the raft partitioning of both PMP22 and MAL and also reduced raft formation in a protein-dependent manner. Class II molecules either increased or decreased raft formation in a manner independent of the presence of PMP22 and MAL. Both classes of compounds altered membrane fluidity in live cells, with no observed toxicity. We further demonstrated that these compounds modulate TRPM8 ion channel function but not phosphorylation of the receptor tyrosine kinase, EGFR. These compounds deepen our understanding of raft biophysics and present a new set of tools for probing lipid raft function.

INTRODUCTION

Lipid rafts are phase-separated domains of the plasma membrane that are thicker and more rigid than the bulk membrane and are typically enriched in cholesterol and phospholipids with saturated acyl chains, often sphingolipids. It has long been theorized that cells utilize lipid rafts as sorting and signaling platforms(1–3). Specific proteins are thought to partition into rafts in cells and facilitate a variety of biological

functions. Rafts have been implicated in immune signaling, neural development, host-pathogen interactions, caveolae, cytoskeletal-membrane contacts, and so forth(4–8). Under physiological conditions lipid rafts in cells are believed to be nanoscale and highly dynamic severely limiting traditional microscopic studies(9–11).

Giant plasma membrane vesicles (GPMVs) derived from the plasma membranes of live cells are a well-established tool for studying lipid rafts and for quantitating the raft affinity of membrane proteins(12). GPMVs are easy to prepare and will spontaneously phase separate into micron-scale liquid ordered (L_o, raft) and liquid disordered (L_d, non-raft) phases. Assorted fluorescent labels are available to label specific phases or protein markers in GPMVs, enabling detection and analysis of lipid phases and resident proteins. GPMVs also retain the lipid and protein composition of the cells plasma membrane from which they are derived(13, 14).

The affinity of a number of membrane proteins for lipid rafts have been assessed in GPMVs. GPMVs have also been used to elucidate the characteristics that drive raft affinity(15–17). The vast majority of membrane proteins that preferentially partition into lipid rafts are single span proteins. The large number of single span raft-avid proteins enabled the identification of structural criteria for raft affinity. Palmitoylation, transmembrane domain length, and surface area are the main drivers of raft partitioning for single-pass membrane proteins(15). No such rules have been determined for multispan proteins in large part because only a small number of raft partitioning multispan proteins have been identified and the rules for single-pass protein do not seem to apply(16, 18).

Peripheral myelin protein 22 (PMP22) is a tetraspan membrane protein that preferentially partitions into lipid rafts. PMP22 is highly expressed in myelinating Schwann cells and is a major component of myelin in the peripheral nervous system (PNS). Duplication of the PMP22 gene causes the most common type 1A form of the peripheral neuropathy, Charcot-Marie-Tooth (CMT) disease(19), a top 10 most common genetic disorder. More severe forms of CMT are caused by certain inherited point mutations in PMP22(20). While the biophysical properties that drive PMP22 into lipid rafts are unknown an analysis of disease-associated PMP22 mutations revealed that most of the mutations examined resulted in reduced preference of the protein for the raft phase versus the disordered phase(18). The fact that the tested disease mutants are known to destabilize folding of the protein suggests raft affinity is dependent on the fold of PMP22(21). Given that PMP22 is thought to be involved in supporting cholesterol homeostasis and trafficking in Schwann cells, it is very possible that its affinity for lipid rafts is closely related to one of its key physiological functions(22). These considerations motivated us to seek new tools for use in elucidating the factors that drive PMP22 raft affinity.

We conducted high throughput screening (HTS) to discover molecules that alter the phase partitioning of PMP22 between ordered and disordered phase domains. Our primary assay reports not only on the phase partitioning of PMP22, but also on whether compounds alter the relative cumulative sizes of ordered (raft) versus disordered phase domains in GPMVs. We here report the discovery of small molecules falling into two classes. Class I compounds decreased lipid raft affinity of PMP22 and MAL [another raft-preferring tetraspan membrane protein(16)] and reduced raft

formation in a protein-dependent manner. Class II compounds altered raft formation independent of proteins. Both classes of compounds were seen to alter membrane fluidity in GPMVs and live cells. We further explored their activities by examining their effects on the activity of the cold sensing TRPM8 channel and epidermal growth factor receptor (EGFR) signaling. These compounds provide new tools for investigating raft dependent phenomena in cells. Additionally, the differing modes of action of these compounds expand our understanding of raft biophysics.

RESULTS

A high-throughput screen identified compounds that alter PMP22 raft affinity

To identify compounds that alter the ordered domain partitioning of PMP22 we conducted a high-throughput screen adapted from our recent method (Fig. 1A)(23). Briefly, GPMVs were made from HeLa cells expressing PMP22. We employed the N41Q (glycosylation deficient) variant of PMP22 since it traffics to the plasma membrane with greater efficiency than wild type but exhibits the same ordered domain preference (18, 24). The disordered phase was labeled with the lipophilic stain DiI while PMP22 was immunolabeled with AlexaFluor 647. GPMVs were deposited into 96 or 384-well plates containing compounds at a final concentration of 10 μM. A 23,360 compound sub-set of the >100,000 compound Vanderbilt Discovery Collection and a library of FDA approved drugs (1,184) were screened. The subset of compounds from the Discovery collection represents a cross-section in terms of the chemical diversity of the master library. Plates were imaged on a high content spinning disc confocal imaging system. VesA software was used to analyze images (23). The power of this approach is

in the number of vesicles that can be imaged and analyzed in an unbiased manner. A typical well results in images containing thousands of GPMVs which are then analyzed automatically, independent of investigator bias or foreknowledge. Hits from the screen were picked using strictly standardized mean difference (SSMD) values on a plate-by-plate basis (typical cutoff was an SSMD value ≥90% of the positive control) based on compound impact on PMP22 $P_{ordered}$. An initial hit rate of 1.06% was observed, resulting in 267 preliminary hits. Hits were then validated in triplicate experiments using compounds from the library. Compounds of interest were then re-ordered from the manufacturer and their effects confirmed. Confirmed compounds were then tested in GPMVs from cells expressing the MAL protein, another lipid raft preferring tetraspan protein(16), rather than PMP22.

Effects of all hits on raft versus ordered phase populations (fraction of GPMVs phase-separated in a field of view) were also measured in GPMVs from both PMP22 and MAL expressing cells. For all confirmed hit compounds (above) we also completed measurements in GPMVs from untransfected cells overexpressing neither PMP22 nor MAL. Hits fell into several distinct categories based on these data. In this work we focus on two interesting classes of compounds.

Protein-dependent modulators of raft affinity and raft stability (Class I molecules)

Among the validated hits, two compounds were found to have unique effects on protein raft affinity and raft stability. VU0615562 and VU0619195 significantly decreased $P_{ordered}$ for both PMP22 and MAL by ~18-20% (Fig. 2 A and B). While PMP22 and MAL are tetraspan myelin proteins with a known affinity for lipid rafts they have little-or-no

sequence homology. These compounds reduce $P_{ordered}$ for two non-homologous tetraspan membrane proteins.

Dose-response experiments indicated that EC_{50} values for the impact of the two compounds on each protein are in the ~1 μM range (Fig 2 C and D). To verify the effects of the compounds are not specific to HeLa cells we confirmed similar activities in GPMVs derived from rat basophilic leukemia (RBL) cells (Supplemental Fig. 1).

We next examined the effects of VU0615562 and VU0619195 on raft stability in GPMVs derived from cells overexpressing PMP22, MAL, or neither protein (untransfected). We used the fraction of phase separated vesicles from images as a proxy for raft stability. The compounds decreased the fraction of phase separated GPMVs in all cases. However, when PMP22 or MAL were overexpressed, this reduction of raft formation was significantly more pronounced compared with GPMVs from untransfected cells (Fig 3 A and B) and was observed across a range of concentrations (Fig. 3D, curve does not approach 0 as in E and F). This led us to speculate that these compounds reduce raft formation via a mechanism that is not specific to a single protein but is dependent on the presence of multiple proteins. We suspected the activity of the compounds in the GPMVs from untransfected cells is because the compounds can exploit endogenous membrane proteins in HeLa cells to exert their effects.

We know that PMP22 expression stabilizes ordered domains(18) in GPMVs so the raft destabilization observed in GPMVs + PMP22 seems to be the consequence of an intrinsic property of VU0615562 and VU0619195 that is somehow enhanced when PMP22 is present. To determine the impact of MAL alone on raft stability we used data from within the same images and compared the fraction of phase separated vesicles

from MAL positive (GFP+) and MAL negative (GFP-) GPMVs (a feature of the VesA software allows us to make this distinction). We used DMSO treated control wells from dose-response experiments for this comparison. In contrast to PMP22(18), we found that MAL expression has very little impact on phase separation (Supplemental Fig. 2). This data indicates that the raft-reducing effects of the compounds with MAL reflect an intrinsic activity of these compounds that is enhanced by the presence of MAL via an unknown mechanism.

To investigate this apparent protein dependence further we tested the impact of these compounds on GPMVs treated with proteinase K. Proteinase K is a broad-spectrum serine protease capable of cleaving proteins preferentially after hydrophobic residues. Note that it has been previously shown that GPMVs can be porous, so it is likely both intracellular and extracellular loops and segments are cleaved by the protease(25). We applied this treatment on GPMVs from untransfected cells because the protease activity would eliminate our ability to label or detect PMP22 or MAL (cleaving the myc tag or GFP fusion), obviating our ability to differentiate GPMVs containing either protein. We found that proteinase K treatment significantly reduced the effects of the compounds (Fig. 3C). This supports the conjecture that the changes induced by the compounds are not specific to any one protein but are dependent on the presence of multiple proteins. The incomplete effect of proteinase K in reducing the raft-lowering activities of these compounds is likely due to its inability to completely digest all membrane proteins present. However, these data combined with the results seen with PMP22 and MAL led us to conclude that multiple proteins somehow enhance the ordered phase-reducing effects of VU0615562 and VU0619195.

To be certain that the compounds were not remodeling the GPMVs we examined the size of GPMVs and the size of the ordered phases when treated with the compounds. Neither GPMV radius nor relative sizes of ordered phase domains were changed by VU0615562 or VU0619195 (Supplemental Fig. 3A and B), even though they decrease the raft affinities of PMP22 and MAL, as well as raft stability.

An examination of the chemical structures of VU0615562 and VU0619195 (Table 1) reveals a Tanimoto coefficient (a metric of chemical similarity ranging from 0-1) of 0.7778(26). This chemical similarity is unsurprising in light of their similar effects on $P_{ordered}$ for PMP22 and MAL, as well as raft stability. Since these compounds were similar, structure activity relationship (SAR) studies were conducted on chemically similar compounds available in the VU Discovery Collection (Supplemental Fig. 4). For VU0615562, seven additional compounds with similar structures (similarity integer value of 97) were tested. For VU0619195, six additional compounds with similar structures (similarity integer value of 85). None of the compounds tested had a greater impact on PMP22 ordered partitioning or raft stability than VU0615562 and VU0619195.

Protein-independent raft modulators (Class II)

It is reasonable to wonder if the protein-dependent raft modulating effects described above for VU0615562 and VU0619195 are unique to these compounds or if all raft modulating compounds would show a similar dependence in their activities on proteins. This turned out not to be the case based on three other compounds discovered in the initial screen for compounds that altered $P_{ordered}$ for PMP22. These compounds have variable effects on ordered partitioning of PMP22 (Fig. 4A) and MAL

(Supplemental Fig. 5A). Two of these compounds—VU519975 and VU607402—decreased phase separation in GPMVs while the FDA-approved drug, PD, increases phase separation (Fig 4B, Supplemental Fig. 1B and 6D). These compounds are diverse (Table 2), exhibiting little structural similarity. Importantly, the presence of PMP22 (Fig. 4B) or MAL (Supplemental Fig. 6B) did not dramatically enhance the effects of these compounds on raft stability. The independence of the activity of the compounds on the presence of proteins is supported by experiments with GPMVs from untransfected cells treated with proteinase K. The activities of these compounds are not sensitive to proteolysis (Fig. 4C). Taken together, we conclude that these compounds are raft modulators that likely interact with the membrane in a protein-independent manner. EC_{50} values for impact on raft stability in GPMVs could not be reliably determined for VU519975 and VU607402 since they were seen to be insoluble in GPMV buffer at concentrations above 15 μM (Fig. 4D). An EC_{50} for the effect of PD on raft stability in GPMVs was determined to be roughly 2.1 μM (Fig. 4E).

Neither VU519975, VU607402, nor PD affect GPMV size or the relative size of raft domains in GPMVs (the fraction of the GPMV that is occupied by PD does induce a small but significant decrease on the size of PMP22-containing ordered domains (Supplemental Fig. 4D-bottom panel and E).

When interpreting any effect on phase separation (raft stability) it is important to factor in the impact of temperature. For example, we found that the impact of PD treatment on raft stability at 27 °C compared to 23 °C was significantly larger (a 125% increase vs a 12% increase) (Supplemental Fig. 6D). See Methods for additional details about this effect.

Both classes of compounds alter membrane fluidity in GPMVs and live cells

We examined the effects of all five compounds (both classes) on membrane fluidity to further characterize their impact on raft stability. Because fluidity experiments can be conducted in live cells this approach also provided an opportunity to connect findings in GPMVs with plasma membranes in living cells. We conducted experiments with Di-4-ANEPPDHQ (Di-4) an environmentally sensitive dye with an emission spectrum that has been demonstrated to report on membrane fluidity(27). Red shifted Di-4 spectra correspond to increases in fluidity and blue shifted spectra corresponds to decreased fluidity.

First, we treated GPMVs derived from HeLa cells incubated with each compound and Di-4 and then measured emission spectra. For the four raft destabilizing compounds, a pronounced red shift from vehicle was observed in micrographs (Fig. 5A) and measured emission spectra (Fig. 5B). To quantify these changes, generalized polarization (GP) values were determined (Fig. 5C). GP values provide a relative means of comparing spectral shifts. For Di-4 emission, lower values correspond to a more red-shifted (more fluid) environment. GP values for the four raft destabilizing compounds indicate a PD, whose effect on increasing raft stability in GPMVs is more modest than the decrease seen for any of the 4 destabilizing compounds, the decrease in fluidity was not significant.

All data presented thus far were collected in GPMVs and therefore do not inform on whether the compounds exert effects in living cells. To address this, we repeated the fluidity measurements with Di-4 in live cells. HeLa cells were treated with compounds

~15 min before a brief incubation with Di-4 to limit internalization of the dye and ensure primarily plasma membrane labeling. Cells were then imaged via laser scanning confocal microscopy using a spectral detector, allowing images from multiple emission wavelengths to be simultaneously acquired (Fig. 5D and Supplemental Fig. 7). GP values were then calculated from the resulting series of images. We found that the changes in GP were very similar to those from GPMVs, with more variability in living cells (Fig. 5E). Two compounds, VU0619195 (class I) and VU0607402 (class II), produced statistically significant increases in membrane fluidity. Methyl-beta-cyclodextrin (MBCD) was included here to deplete membranes of cholesterol and increase membrane fluidity. Interestingly, the effect of MBCD treatment was modest in comparison to VU0619195 and VU0607402. The effects and effects sizes of VU0615562, VU0519975, and PD on Di-4 emission in live cells while not significant show similar changes relative to each other as in the GPMV Di-4 experiments.

Qualitatively, the MBCD treated cells also appeared rounded (Supplemental Fig. 7, bottom row) compared to the hit compound treated cells, which retained the well spread appearance of untreated cells, suggesting that the compounds presented here are better tolerated by live cells than MBCD treatment. Trypan blue cell viability experiments confirmed that MBCD shows toxicity in cells while none of the 5 compounds of this work were cytotoxic (Supplemental Fig. 7B). VU0619195 and VU0607402 may, therefore, provide improved tools for manipulating lipid rafts in living cells in studies of the functional relevance of lipid rafts in different biological processes. Knowing that the effects of the compounds discovered in this work extend to the plasma

membranes of living cells, we were motivated to investigate their impact on putative raft-dependent functions of selected membrane proteins.

Compounds alter TRPM8 activity but not EGFR phosphorylation

To test if the compounds could alter a biological outcome that is thought to be influence by lipid rafts, we examined their effects on TRPM8 ion channel function. TRPM8 is a cold and menthol sensing ion channel(28, 29). Many ion channels, including TRPM8 are thought to associate with lipid rafts and have signaling properties that are sensitive to being in or out of rafts(30, 31). We conducted automated patch clamp (APC) electrophysiology experiments (Fig. 6A, Supplement Figure 7A) to determine if treatment of our compounds altered TRPM8 channel activity. Patched cells were equilibrated to 30 °C, similar to a previous study, and treated with menthol (a TRPM8 agonist) before and after a brief perfusion (15 min) with the compounds (32). Comparisons of the post-treatment response were then made to the pre-treatment response. As with the fluidity experiments, MBCD was included as a control since previously published studies used MBCD to deplete cholesterol and disrupt lipid rafts. We found that perfusion with VU0619195 (Class I) and VU0607402 (Class II) both decreased the response of TRPM8 to menthol stimulation as did MBCD (Fig. 6B, Supplemental Figure 7B). This result suggests that decreased lipid raft formation correlates with reduced TRPM8 channel activity. PD, (Class II, increases raft formation) did not significantly alter TRPM8 activity. These results are similar to those seen in the live-cell fluidity experiments providing an important cross validation.

Cell surface TRPM8 was quantified via flow cytometry, showing that the effects of the compounds are not due to decreased levels of the protein at the plasma membrane (Supplemental Figure 8C). Interestingly, MBCD increased the level of surface TRPM8, which may be a consequence of its known activity as an endocytosis inhibitor(33).

We also examined the impact of compounds on activation of the epidermal growth factor receptor (EGFR) by epidermal growth factor (EGF). Previous studies have shown changes in EGFR activation following disruption of lipid rafts by MBCD treatment(34–36). We treated HeLa cells with VU0619195, VU0607402, or PD for 15 minutes (as in the TRPM8 experiments) prior to a brief (1 min) treatment with EGF. Cells were then lysed and levels of EGFR phospho-tyrosine 1173 and phospho-ERK (which is phosphorylated downstream of EGFR phosphorylation) were quantified via Western blot analysis. We did not see significant effects on either EGFR or ERK phosphorylation (Fig. 6C, Supplemental Fig. 9), indicating that these signaling processes are not sensitive to short-term changes in membrane fluidity or raft modulation. These data also indicate that not all plasma membrane signaling events are sensitive to the changes in lipid raft stability induced by these compounds. These data therefore also provide a useful counterexample to the findings with TRPM8.

DISCUSSION

HTS led to the discovery of five novel lipid raft modulating small molecule compounds: two protein-dependent raft destabilizers that also reduced the lipid raft affinity of both PMP22 and MAL (class I) and two protein-independent raft destabilizers and one protein-independent raft stabilizer that promotes the lipid raft affinity of PMP22 and MAL

(class II). The compounds exerted effects both in isolated plasma membrane vesicles and in live-cell plasma membranes. They also altered the signaling of a raft-sensitive ion channel TRPM8.

Commonly used methods of altering lipid rafts in cells include removal or delivery of cholesterol via MBCD and use of alcohols of varying chain lengths. These approaches each have limitations. MBCD efficiently removes cholesterol, but this is ultimately lethal to cells. MBCD is also not specific and removes phospholipids as well as cholesterol(37). Hexadecanol and octanol can be used to decrease or increase membrane fluidity respectively but have low miscibility in aqueous buffers and media making them challenging to work with in cell-based assays. We also recently described bioactive lipid-like compounds that alter phase separation, but these are all known to have effects on various cellular functions for which they were originally described (for example, one hit is a known protease inhibitor) (23). Here we have presented new small molecules, two of which induce a more robust increase in membrane fluidity than MBCD while all the compounds described here remained non-toxic. These compounds are therefore useful tools for manipulating lipid rafts and raft proteins in biophysical and cell biological studies.

Potential applications for these compounds are exemplified in our studies with TRPM8 and EGFR. Prior studies implicated lipid raft localization as having regulatory effects on the activities of both TRPM8 and EGFR(34, 35, 38). Our results showed that compounds that decrease raft formation robustly decrease TRPM8 signaling. We note that previous studies reported an *increase* in rat TRPM8 channel activity after treatment with MBCD (32, 39). The difference in phenotype could be the result of speciation

difference between the human TRPM8 used in this study compared to the rat TRPM8 used in the previous studies. Speciation differences have been seen in TRP channels including TRPA1, TRPV3, and TRPV1(40). Clinical trials involving the heat sensor TRPV1 have faced setbacks, partly due to how TRPV1 antagonists differentially affect thermoregulation and thermosensing between rat and humans(41).

Reduced raft formation induced by treatment with the same compounds that affected TRPM8 had little to no effect on EGFR phosphorylation, in contrast to the reported impact of lipid raft disruption by MCBD treatment(34, 35, 42). This suggests that EGFR activity may be more sensitive to the cholesterol concentration in the membrane than it is to lipid rafts. Some G protein-coupled receptors are known to be allosterically regulated by direct binding of cholesterol, for example(43). Prior work on the yeast transcriptional regulator Mga2, for example, has demonstrated that some proteins sense acyl chain composition rather than overall fluidity and respond with a rotational conformational change to regulate their activity(44).

Further studies will need to be conducted to establish the exact mechanisms by which the five compounds reported in this work exert their effects. The data suggest that the two Class I protein-dependent compounds work to change protein raft affinity and phase separation by altering protein-lipid interactions. They may intercalate into the membrane at protein lipid-interfaces and disrupt raft promoting interactions. The discovery of these compounds supports previous assertions that proteins play a critical role in regulating lipid rafts(45). The three Class II protein independent compounds likely work by inserting into the membrane and altering lipid packing to cause the fluidity changes reported on by the Di-4 assays. We do not have reason to suspect that these

compounds change the lipid composition (as MBCD does) on the short time scales (15 minutes) they were tested, given their structures. However, lipidomic analyses will need to be conducted to rule this out. We do think it is likely that a long-term incubation of live cells with the compounds could result in some level of membrane remodeling as cells respond to the changes in raft stability and membrane fluidity. Cells have adapted mechanisms to sense and respond to these changes that result from natural temperature changes which are believed to keep their membranes near the miscibility critical point (46–49). Further experiments with the compounds can broaden our understanding of these mechanisms.

Overall, the discovery of these two classes of compounds shed light on the fact that there are likely both protein-lipid and lipid-lipid interactions stabilizing lipid rafts and that these can be independently manipulated. These compounds also present new tools for interrogating lipid rafts and raft proteins in cells that can provide alternative or complementary approaches to existing methods.

METHODS

Cell culture

HeLa and RBL-2H3 cells and were acquired from the American Tissue Culture Collection (ATCC, Manassas Va, cat #CCL-2 and CRL-2256). T-REx-293 cells were acquired from Invitrogen (Cat # R71007). Cells were grown at 37 °C in 5% CO_2 in a humidified incubator. HeLa cells were cultured in low glucose DMEM (Gibco # 11885084) supplemented with 10% fetal bovine serum (FBS, Gibco, #26140-079) and 1% penicillin/streptomycin (P/S, Gibco, #15140-122). RBL-2H# cells were cultured in

MEM (Gibco 11095808) with 10% FBS and 1% penicillin/streptomycin. T-Rex-293 cells were cultured in high glucose DMEM (Gibco cat # 11965092) supplemented with 10% tetracycline free fetal bovine serum (Corning cat # 35-075-CV) with 1% penicillin/streptomycin.

GPMV formation and imaging

HeLa cells were plated at ~1.4 x 10^6 cells total in a 150 mm plate. For PMP22 experiments: 24 hrs later cells were transfected with 15 ug of pSF PMP22 N41Q-myc using Fugene 6 (Promega cat # E2691) following the manufacturers protocol. Cells were grown for an additional 48 hrs post transfection. GPMVs were generated using a standard protocol(12), cells were first rinsed twice with 10 ml of inactive GPMV buffer (150 mM NaCl, 10 mM HEPES, 2 mM CaCl2, pH7.4). To label the disordered phase, cells were stained with DiIC12(3) (1,1'-Didodecyl-3,3,3',3'-Tetramethylindocarbocyanine Perchlorate) (DiI, Invitrogen cat # D383) for 10 minutes. Cells were then rinsed twice again with inactive GPMV buffer then subsequently incubated in 8.5-10 ml of active GPMV buffer (GPMV buffer + 2 mM DTT, 25 mM formaldehyde) at 37°C for 1.5 hrs. After incubating, GPMVs in solution were collected from the dish and allowed to settle at room temperature for 1 hr. 8-9 mL of GPMVs were then collected by pipetting from neither the top nor the bottom of the tube to leave behind both floating and settled debris. A mouse anti-myc antibody (Cell Signaling, 9B11) was then added at a ratio of 1:1500 and incubated for 1 hr. This was followed by incubation with an anti-mouse antibody conjugated to AlexaFluor647 (Cell Signaling, cat # 4410) at 1:15000. GPMVs were added to multi-well plates with compounds from DMSO stocks and allowed to

incubate for 1.5 hrs. Plates were then imaged on an ImageXpress Micro Confocal High Content Screening System (Molecular Devices, San Jose CA) with a Nikon 40X 0.95 NA Plan Apo Lambda objective and an Andor Zyla 4.2MP 83% QE sCMOS camera, and an 89-North LDI 5 channel laser light source.

High-throughput screen and GPMV image analysis

A pilot screen was conducted with an FDA approved drug library (1,184 compounds) by testing the library plated in triplicate. Primaquine diphosphate (PD) was found to have significant effects on promoting PMP22 ordered partitioning and increasing raft stability. It was carried through the larger screen as a positive control. Compounds were obtained from the Vanderbilt Discovery collection at the VU HTS core. This library contains over 100,000 compounds with the first 20,000 representing the greatest structural diversity. Compounds were dispensed via a Labcyte Echo 555 into 384-well plates such that final the final screening concentration for all compounds was 10 μM. GPMVs were made and labeled as described above and added to the plates containing compounds. The first and last columns of the plates were filled with positive and negative controls. Plates were incubated for at least 1.5 hours at room temperature prior to imaging. 16 images per well were collected using an IXMC as described above. Images were then analyzed using VesA. Strictly standardized mean differences (SSMDs) were used to calculate effect sizes for the PMP22 ordered phase partition coefficient ($P_{ordered}$), for every well(50, 51). The SSMDs for positive (PD) and negative (DMSO) controls were used as a benchmark to select hits from each plate. A typical cutoff for selecting hits was a SSMD value of >90% of the positive control SSMD for

PMP22 ordered partitioning. These criteria resulted in a 1-3% hit rate. SSMD values for PMP22 ordered partitioning were used to pick hits. For each hit we also noted the fraction of phase separated vesicles (also calculated by VesA). A minimum of 100 GPMVs expressing PMP22 per well was required to be included as a hit. Hits were then screened by qualitatively assessing the images from screening. Hits that showed significant visible compound precipitation or extreme changes in GPMV size/shape were discarded. After screening 23,360 compounds 267 hits were identified following the above criteria, reflecting a 1.06% hit rate. These hits were then tested in triplicate against library compound. From hits that were validated at this phase, those with the largest effects were selected and reordered (20 compounds).

Experiments using reordered compounds were conducted in 96-well plate with duplicate or triplicate wells (technical replicates) in each plate (biological replicate). For experiments with PMP22, MAL or GPI-GFP only GPMVs containing the overexpressed construct were analyzed. For follow-up and dose response experiments, a minimum of 10 phase separated GPMVs per biological replicate were required for ordered partitioning measurements (determination of $P_{ordered}$). For experiments without PMP22, MAL, or GPI-GFP (untransfected cells) all GPMVs were analyzed.

Compound repurchasing

Compounds from the Vanderbilt Discovery Collection were reordered from Life Chemicals (VU0615562, Cat. No. F3382-6184) (VU0619195, Cat. No. F3398-2024) (VU0519975, Cat No. F5773-0110) (VU0607402, Cat. No. F3255-0148) (Niagara on the

Lake, Ontario, Canada). PD was acquired from Selleckchem (Cat. No. S4237) (Houston, TX, USA).

Dose-response experiments

GPMVs from cell expressing or not expressing PMP22 or MAL were made and labeled as described above. Doses of hit compounds or DMSO were made by serial dilution and deposited into wells of a 96-well plate for a final concentration from 0.01 to 15 μM. The measured fraction of phase separated GPMVs and $P_{ordered}$ were normalized to DMSO controls and averaged. Curves were fit in GraphPad Prism10 and half maximal effective concentrations (EC50) were determined using a non-linear sigmoidal model.

Proteinase K treatment

GPMV protease treatment was conducted as previously described(52). GPMVs were made from untransfected HeLa as described above and labeled with DiD and NBD-PE. GPMVs were then separated into 2 tubes. One tube was treated with 20 μg/mL of Proteinase K (Macherey-Nagel cat #740506). Proteinase K and untreated GPMVs were incubated for 45 min at 37° C. 2 mM PMSF was added to quench the proteinase K treatment. GPMVs were then added to wells in a 96-well plate containing compounds for a final concentration of 10 μM. GPMVs were imaged and analyzed as described above.

Temperature Considerations in GPMVs

With the following exception, all of the work presented thus far was carried about at 21-23 °C. Phase separation is highly temperature dependent and previous work found that

the temperature at which half of GPMVs from HeLa cells phase separate is roughly 25 °C(18). The instrument used for most of this work is limited at low end of temperature to about 21°C. So, we could not easily probe the effect size of raft destabilizing compounds by further decreasing the temperature (which would increase phase separation). Our ability to heat samples was less restricted. In addition to the altered effects on raft stability in response to PD treatment, there was also a more modest increase in MAL ordered partitioning at 27 °C vs 23 °C (Supplemental Fig. 6C). This illustrates that temperature is a crucial variable to consider when interpreting the effects of these compounds on raft stability and ordered partitioning. We next wondered about how the compounds affect live cells.

Plate reader membrane fluidity assay

For fluidity measurements in GPMVs, GPMVs were made as described above without any staining prior to vesiculation. Once collected and settled, GPMVs were stained with Di-4 -ANEPPDHQ (Invitrogen, cat # D36802). To optimize the concentration of each stain a pilot study was conducted with 0.1% DMSO and single compound and dye concentrations ranging from 0.5 μM to 10 μM. From this, 1 μM as determined to give the best effect sizes for Di-4. For experiments with all compounds GPMVs were treated with dye then deposited in wells of a 96-well plate with compounds (10 μM final for each compound) and incubated at room temperature for about 40 minutes. After incubation the plate was read on a SpectraMax iD3 plate reader (Molecular Devices). Data were acquired using SoftMax Pro 7 version 7.1.0 (Molecular Devices). Di-4 was excited at 470 nm and emission spectra were collected from 550 to 800 nm using 2 nm steps. The

photomultiplier tube gain was set to automatic with an integration time of 140 ms. From the spectra, generalized polarization values were calculated with the following formula:

$$GP = \frac{I_B - I_R}{I_B + I_R}$$

Where I_B is a value in the blue end of the emission spectra and I_R is a value at the red end. For Di-4 565 nm and 605 nm were selected for I_B and I_R respectively.

Image-based membrane fluidity assays

For imaging, GPMVs were prepared, treated with compounds, and labeled with Di-4 in the same manner as described in the previous section. They were seeded in an 8-well chamber slide with a coverslip on the bottom (Ibidi cat # 80806). Images were acquired on a Zeiss LSM 880 laser scanning confocal using a spectral detector and a 40X oil immersion objective. Images were collected at emission wavelengths from 410 nm to 689.5 nm at an interval of 8.9 nm.

Live-cell experiments were conducted by first seeding 10,000 cells per well in 8-well chamber slides. The following day, 1 hr prior to imaging, cells treated to deplete cholesterol were first rinsed with serum-free media then incubated with 10 mM methyl-ß-cyclodextrin (MBCD) in serum-free DMEM. After 30 minutes at 37 C, cells were removed from the incubation and treated with 10 μM compounds in serum-free CO_2 independent media (Gibco L15 media, # 2108302) for 30 min. (MBCD treated well was also swapped from 10 mM MBCD in serum-free CO_2 independent media). Prior to imaging, Di-4 was added to a final concentration of 2 μM. Imaging and Di-4 addition were staggered to ensure less than 30 min passed after addition of the dye and imaging. This is in line with previous observations that Di-4 begins to accumulate in

endosomes after 30 min. Additionally, images were acquired at room temperature to slow internalization of the dye. Imaging was conducted on the LSM 880 as described in the previous section. Fluorescence intensities of individual cells were measured in ImageJ across all 32 wavelengths. 2 to 3 cells were measured using Fiji (53) from 5 fields of view per condition. GP values were calculated as they were in the plate reader assay with intensities 561.5 nm and 605.8 nm used at the blue and red values respectively.

Automated patch clamp electrophysiology

HEK293 cells stably expressing full-length human TRPM8 were grown in DMEM media (Gibco 11960077) with 10% fetal bovine serum (Gibco 16000), 4 mM L-glutamine (Gibco 25030), 100 U/mL penicillin-streptomycin (Gibco 15140), 100 μM non-essential amino acid solution (Gibco 11140050), 4 mM glutaMax (Gibco 35050061), 200 μg/mL G418 (Sigma-Aldrich A1720), and 0.12% sodium bicarbonate (Gibco 25080094) at 37 °C and 8% CO2 in 100 mm dishes, as done previously(54). After growing for 3-4 days to 75% confluency, the cells were washed twice with 2 mL per dish of phosphate buffer saline solution (PBS), pH 7.4 (Gibco 10010031) and allowed to incubate in 2 mL per dish of accutase (Gibco A1110501) for 5 minutes at 37 °C. Cells were then triturated into a conical tube and centrifuge at 200 ×g for 1.5 minutes to remove the accutase. The cells were resuspended with serum-free media (Gibco 11686029) and transferred into a T25 flask. The cells were allowed to recover by placing the cells onto an orbital shaker at 50 rpm for at least 30 minutes at room temperature. The cells were then centrifuged again at 200 x g for 1.5 minutes and resuspended in extracellular buffer (10 mM

HEPES, 145 mM NaCl, 4 mM KCl, 1 mM MgCl2, 2 mM CaCl2, 10 mM glucose, pH 7.4) to a cell density of 3-7 × 106 cells/mL. The osmolality of the extracellular buffer was adjusted using a Vapro 5600 vapor pressure osmometer (Wescor) with sucrose to 315-330 mOSm and pH using NaOH.

Data was collected using IonFluxMercury HT (Cell Microsystems) with Ionflux HT v5.0 software using ensemble IonFlux Plate HT (Cell Microsystems 910-0055). The ensemble plates consist of 64 amplifiers with each amplifier being able to record 20 cells at once and the 20 cells are summed for each amplifier. On the plate, the amplifiers were filled with intracellular solution (10 mM HEPES, 120 mM KCl, 1.75 mM MgCl2, 5.374 mM CaCl2, 10 mM EGTA, 4 mM NaATP, pH 7.2. Osmolality was adjusted with sucrose to 305-315 mOsm and the pH was adjusted using KOH. Compounds were dissolved into DMSO before adding to extracellular solution, where the 0.03% DMSO was kept consistent across all compounds and controls. A water rinse protocol from Cell Microsystems was ran on the ensemble plate before the experiment. The protocol for the experiment is divided into four steps: prime, trap, break, and data acquisition. During the prime step: (1) the main channel was applied 1 psi for t = 0-25 s and 0.4 psi for t = 25-60 s (2) the trap and compound channels were applied at 5 psi for t = 0-20 s and then 1.5 psi for t = 20-55 s followed by only the traps at 2 psi for t = 55-60 s. For the voltage during the prime step, a pulse was applied every 150 ms, where the 0 mV holding potential was applied during t = 0-50 ms, 20 mV was applied during the t = 50-100 ms, and 0 mV during the t = 100-150 ms. During the trap step: (1) the main channel is applied 0.1 psi for t = 0-5 s before applying 0.5 s pulses of 0.2 psi every 5 s during t = 5-135 s (2) the trap channel is applied 6 inHg for t = 0-135 s. For the voltage during the

trap step, a pulse was applied every 70 ms, where the -80 mV holding potential was applied between t = 0-20 ms, -100 mV for t = 20-50 ms, -80 mV for t = 50-70 ms. During the break step: (1) the main channel is applied 0.1 psi for t = 0-100 s (2) the trap channel was applied 6 inHg between t = 0-10 s, vacuum ramp from 10 to 14 inHg from t = 10-40 s, and 6 inHg for t = 40-100 s. For the voltage during the break step, a pulse was applied every 150 ms, where -80 mV holding potential was applied between t = 0-50 ms, -100 mV for t = 50-100 ms, and -80 mV for t = 100-150 ms. During the data acquisition: (1) the main channel is applied at 0.15 psi for t = 0-1350 s and 0 psi for 1350-2450 s, (2) the traps channel is applied 5 inHg for t = 0-3 s, 3 inHg for t = 3-1350 s, and 0 inHG for t = 1350-2450 s. For the voltage during the data acquisition, a pulse was applied every 625 ms, where the -60 mV holding potential was applied between t = 0-100 ms, -70 mV for t = 100-200 ms, -60 mV for t = 200-300 ms, a voltage ramp from -120 mV to 160 mV for t = 300-525 ms and -60 mV for t = 525-625 ms. No perfusion were flowed during the first 5 minutes of the experiment to allow the plate to equilibrate to 30 °C. Menthol was perfused for 75 s for four times at the start to get an initial current response before applying the compounds for 15 minutes followed by two 75 s perfusions of menthol with compound.

Ionflux Data Analyzer v5.0 was used to analyze the data. Leak subtraction was performed on the data based on the -60 mV initial holding potential and -70 mV voltage steps from the data acquisition. Each point of the current trace is from the difference of the current at 120 mV and the holding potential at -60 mV. The data was averaged from 7 points after 25 s of perfusion of menthol without or with the compound. The last two menthol perfusions before the application were then averaged and compared to the two

menthol perfusions after application of the compound to determine the ratio of menthol response.

Trypan blue cell viability

To ensure that effects seen in Di-4 live cell fluidity experiments and APC experiments were not due to inherent toxicity of the compounds trypan blue experiments were conducted. HeLa cells were collected and treated with 10 μM compound or 10 mM MBCD as in the Di-4 assay. Live-dead staining was then conducted with trypan blue as previously described (55). Cells were mixed in a 50:50 ratio with trypan clue reagent then immediately quantified on an automated Countess 3 cell counter (Fisher Scientific). Experiments were conducted on three separate days with measurements taken in duplicate.

TRPM8 cell surface measurements

TRPM8 stable cells were cultured as described above. Cells were collected by dissociation with 0.5 mM EDTA in PBS and resuspended in media. Cells were then incubated in 100 μl of media with 10 μM compound or 10 mM MBCD for 15 minutes as in the electrophysiology experiments. Cells were then fixed with 100 μl Buffer A from a Fix & Perm kit for flow cytometry (Invtitrogen, Cat. No. GAS004). Cells were then rinsed 3 times in flow cytometry buffer (PBS + 5% FBS + 0.1% NaN_3). Cells were then labeled with either of two TRPM8 primary antibodies targeted to an extracellular epitope (Alomone, Cat. No. ACC-049 Abcepta, Cat. No. AP8181D). The Alomone antibody was used at a dilution of 1:100 while the Abcepta antibody was used at a dilution of 1:50 for

1 hr in the flow cytometry buffer. Cells were rinsed 3 times again then labeled with an anti-Rabbit-AlexaFlour488 secondary at a 1:1000 dilution (Cell Signaling, Cat. No. 4412) for 45 min. Cells were rinsed 3X again and resuspended in a final volume of 300 µl. Single cell fluorescence intensities were measure on a BD Fortessa 5-laser analytical cytometer. Geometric means of the resulting intensity distributions were calculated in FlowJo (version 10). Statistical comparisons were made in GraphPad Prism (version 10).

Immunoblotting to detect EGFR activation

For EGFR activation studies, adherent HeLa cells at 70 % confluency in a 60 mm dish were starved overnight (~18 hr) with starvation media - serum free DMEM/F12 (Gibco) media supplemented with only Pen-Step. Starved cells were exposed to small molecules of interest by replacing the overnight starvation media with 4 mL of pre-warmed starvation media containing 10 µM small molecule of interest and 0.1 % DMSO (Cell Signaling Technologies) for noted times at 37 °C. After incubation, EGFR was activated with the addition of 1 mL of pre-warmed starvation media containing 500 ng/mL EGF (R&D Systems) for 1 minute. Due to the speed of EGFR activation kinetics in HeLa cells, treated plates were then flash frozen in liquid nitrogen after media removal. Frozen plates were then placed on ice and lysed with scraping in ice-cold RIPA lysis buffer supplemented with PhosStop phosphatase inhibitor and Complete protease inhibitor (Roche). Lysates were clarified by centrifugation and subjected to immunoblotting using NuPage Novex 4 % - 12 % Bis-Tris Protein Gels (ThermoFisher Scientific). After electrophoresis, intact gels were transferred to Immoblion-P PVDF

(Millipore) membranes and cut into three horizontal strips guided by Precision Plus molecular weight ladder (Bio-Rad) and incubated overnight in blocking buffer - 20 mM Tris, 150 mM NaCl, 0.1 % Tween-20 (Bio-Rad) pH 7.6 (TBST) with 3 % w/v Bovine Serum Albumin Fraction V (Fisher Bioreagents). Primary rabbit antibodies against EGFR pY1173 (53A5, 3972S), phospho-p44/42 MAPK – also known as ERK 1/2 (9101S), and GRB2 (3972S) were purchased from Cell Signaling Technology and used at a dilution of 1:1000 in TBST for 1 hr at RT with gentle agitation. Goat anti-rabbit IgG (H+L) conjugated to horse radish peroxidase (ThermoFisher Scientific, 31460) with glycerol was used at a dilution of 1:5000 for 1 hr in blocking buffer with gentle agitation. Blots were detected using SuperSignal West Pico Chemiluminescent Substrate (ThermoFisher Scientific) on a LI-COR 2800 using the chemiluminescent and 700 nm channels to detect antibody and molecular weight bands signals, respectively. Chemiluminescent signal was checked for saturation and bands of interest were integrated with Image Studio (LI-COR, version 3.1).

FUNDING

HTS core instruments were funded by 1S10OD021734. We acknowledge the support from the US NIH grants R01 NS095989 (C.R.S.), R35 GM141933 (W.D.V.H.), and F32 GM151766 (JMH), as well as by a grant from the CMT Research Foundation (C.R.S.). The content is solely the responsibility of the authors and does not necessarily represent the official views of any funding agencies.

Acknowledgements

Some experiments were performed in the Vanderbilt High-Throughput Screening (HTS) Core Facility with assistance provided by Tom Hasaka and Corbin Whitwell. The FDA approved library was provided by the Vanderbilt CTSA (UL1TR00044) and distributed by the Vanderbilt High-Throughput Screening Core Facility as was the Vanderbilt Discovery Collection. The HTS Core receives support from the Vanderbilt Institute of Chemical Biology and the Vanderbilt Ingram Cancer Center (P30 CA68485).

References

1. Lingwood, D., and Simons, K. (2010) Lipid rafts as a membrane-organizing principle. *Science (1979)*. **327**, 46–50
2. Staubach, S., and Hanisch, F. G. (2011) Lipid rafts: signaling and sorting platforms of cells and their roles in cancer. *Expert Rev Proteomics*. **8**, 263–277
3. Tsui-Pierchala, B. A., Encinas, M., Milbrandt, J., and Johnson, E. M. (2002) Lipid rafts in neuronal signaling and function. *Trends Neurosci*. **25**, 412–417
4. Varshney, P., Yadav, V., and Saini, N. (2016) Lipid rafts in immune signalling: current progress and future perspective. *Immunology*. **149**, 13–24
5. Viljetić, B., Blažetić, S., Labak, I., Ivić, V., Zjalić, M., Heffer, M., and Balog, M. (2024) Lipid Rafts: The Maestros of Normal Brain Development. *Biomolecules 2024, Vol. 14, Page 362*. **14**, 362
6. Mañes, S., Del Real, G., and Martínez-A, C. (2003) Pathogens: raft hijackers. *Nature Reviews Immunology 2003 3:7*. **3**, 557–568
7. Parton, R. G., and Richards, A. A. (2003) Lipid Rafts and Caveolae as Portals for Endocytosis: New Insights and Common Mechanisms. *Traffic*. **4**, 724–738
8. Head, B. P., Patel, H. H., and Insel, P. A. (2014) Interaction of membrane/lipid rafts with the cytoskeleton: Impact on signaling and function: Membrane/lipid rafts, mediators of cytoskeletal arrangement and cell signaling. *Biochimica et Biophysica Acta (BBA) - Biomembranes*. **1838**, 532–545
9. Pralle, A., Keller, P., Florin, E. L., Simons, K., and Hörber, J. K. H. (2000) Sphingolipid–Cholesterol Rafts Diffuse as Small Entities in the Plasma Membrane of Mammalian Cells. *Journal of Cell Biology*. **148**, 997–1008
10. Bolmatov, D., Soloviov, D., Zhernenkov, M., Zav'Yalov, D., Mamontov, E., Suvorov, A., Cai, Y. Q., and Katsaras, J. (2020) Molecular Picture of the Transient Nature of Lipid Rafts. *Langmuir*. **36**, 4887–4896
11. Janosi, L., Li, Z., Hancock, J. F., and Gorfe, A. A. (2012) Organization, dynamics, and segregation of Ras nanoclusters in membrane domains. *Proc Natl Acad Sci U S A*. **109**, 8097–8102
12. Sezgin, E., Kaiser, H. J., Baumgart, T., Schwille, P., Simons, K., and Levental, I. (2012) Elucidating membrane structure and protein behavior using giant plasma membrane vesicles. *Nat Protoc*. **7**, 1042–1051
13. Fridriksson, E. K., Shipkova, P. A., Sheets, E. D., Holowka, D., Baird, B., and McLafferty, F. W. (1999) Quantitative analysis of phospholipids in functionally important membrane domains from RBL-2H3 mast cells using tandem high-resolution mass spectrometry. *Biochemistry*. **38**, 8056–8063
14. Bauer, B., Davidson, M., and Orwar, O. (2009) Proteomic Analysis of Plasma Membrane Vesicles. *Angewandte Chemie*. **121**, 1684–1687
15. Lorent, J. H., Diaz-Rohrer, B., Lin, X., Spring, K., Gorfe, A. A., Levental, K. R., and Levental, I. (2017) Structural determinants and functional consequences of protein affinity for membrane rafts. *Nature Communications 2017 8:1*. **8**, 1–10

16. Castello-Serrano, I., Lorent, J. H., Ippolito, R., Levental, K. R., and Levental, I. (2020) Myelin-Associated MAL and PLP Are Unusual among Multipass Transmembrane Proteins in Preferring Ordered Membrane Domains. *J Phys Chem B*. **124**, 5930–5939
17. Levental, I., Lingwood, D., Grzybek, M., Coskun, Ü., and Simons, K. Palmitoylation regulates raft affinity for the majority of integral raft proteins. 10.1073/pnas.1016184107/-/DCSupplemental
18. Marinko, J. T., Kenworthy, A. K., and Sanders, C. R. (2020) Peripheral myelin protein 22 preferentially partitions into ordered phase membrane domains. *Proceedings of the National Academy of Sciences*. **117**, 14168–14177
19. Divincenzo, C., Elzinga, C. D., Medeiros, A. C., Karbassi, I., Jones, J. R., Evans, M. C., Braastad, C. D., Bishop, C. M., Jaremko, M., Wang, Z., Liaquat, K., Hoffman, C. A., York, M. D., Batish, S. D., Lupski, J. R., and Higgins, J. J. (2014) The allelic spectrum of charcot–marie–tooth disease in over 17,000 individuals with neuropathy. *Mol Genet Genomic Med*. **2**, 522–529
20. Li, J., Parker, B., Martyn, C., Natarajan, C., Guo, J., Li, J., Parker, : B, Martyn, : C, Natarajan, C., and Guo, J. (2012) The PMP22 Gene and Its Related Diseases. *Molecular Neurobiology 2012 47:2*. **47**, 673–698
21. Schlebach, J. P., Narayan, M., Alford, C., Mittendorf, K. F., Carter, B. D., Li, J., and Sanders, C. R. (2015) Conformational Stability and Pathogenic Misfolding of the Integral Membrane Protein PMP22. *J Am Chem Soc*. **137**, 8758–8768
22. Stefanski, K. M., Wilkinson, M. C., and Sanders, C. R. (2024) Roles for PMP22 in Schwann cell cholesterol homeostasis in health and disease. *Biochem Soc Trans*. **52**, 1747–1756
23. Fricke, N., Raghunathan, K., Tiwari, A., Stefanski, K. M., Balakrishnan, M., Waterson, A. G., Capone, R., Huang, H., Sanders, C. R., Bauer, J. A., and Kenworthy, A. K. (2022) High-Content Imaging Platform to Discover Chemical Modulators of Plasma Membrane Rafts. *ACS Cent Sci*. **8**, 370–378
24. Marinko, J. T., Wright, M. T., Schlebach, J. P., Clowes, K. R., Heintzman, D. R., Plate, L., and Sanders, C. R. (2021) Glycosylation limits forward trafficking of the tetraspan membrane protein PMP22. *Journal of Biological Chemistry*. 10.1016/j.jbc.2021.100719
25. Skinkle, A. D., Levental, K. R., and Levental, I. (2020) Cell-Derived Plasma Membrane Vesicles Are Permeable to Hydrophilic Macromolecules. *Biophys J*. **118**, 1292–1300
26. Bajusz, D., Rácz, A., and Héberger, K. (2015) Why is Tanimoto index an appropriate choice for fingerprint-based similarity calculations? *J Cheminform*. **7**, 1–13
27. Jin, L., Millard, A. C., Wuskell, J. P., Dong, X., Wu, D., Clark, H. A., and Loew, L. M. (2006) Characterization and Application of a New Optical Probe for Membrane Lipid Domains. *Biophys J*. **90**, 2563–2575
28. Peier, A. M., Moqrich, A., Hergarden, A. C., Reeve, A. J., Andersson, D. A., Story, G. M., Earley, T. J., Dragoni, I., McIntyre, P., Bevan, S., and Patapoutian, A. (2002) A TRP Channel that Senses Cold Stimuli and Menthol. *Cell*. **108**, 705–715
29. McKemy, D. D., Neuhausser, W. M., and Julius, D. (2002) Identification of a cold receptor reveals a general role for TRP channels in thermosensation. *Nature 2002 416:6876*. **416**, 52–58

30. Martens, J. R., O'Connell, K., and Tamkun, M. (2004) Targeting of ion channels to membrane microdomains: Localization of K V channels to lipid rafts. *Trends Pharmacol Sci*. **25**, 16–21
31. Bobkov, D., and Semenova, S. (2022) Impact of lipid rafts on transient receptor potential channel activities. *J Cell Physiol*. **237**, 2034–2044
32. Morenilla-Palao, C., Pertusa, M., Meseguer, V., Cabedo, H., and Viana, F. (2009) Lipid Raft Segregation Modulates TRPM8 Channel Activity. *Journal of Biological Chemistry*. **284**, 9215–9224
33. Dutta, D., and Donaldson, J. G. (2012) Search for inhibitors of endocytosis. *Cell Logist*. **2**, 203–208
34. Lambert, S., Vind-Kezunovic, D., Karvinen, S., and Gniadecki, R. (2006) Ligand-Independent Activation of the EGFR by Lipid Raft Disruption. *Journal of Investigative Dermatology*. **126**, 954–962
35. Irwin, M. E., Mueller, K. L., Bohin, N., Ge, Y., and Boerner, J. L. (2011) Lipid raft localization of EGFR alters the response of cancer cells to the EGFR tyrosine kinase inhibitor gefitinib. *J Cell Physiol*. **226**, 2316–2328
36. Chen, X., and Resh, M. D. (2002) Cholesterol Depletion from the Plasma Membrane Triggers Ligand-independent Activation of the Epidermal Growth Factor Receptor. *Journal of Biological Chemistry*. **277**, 49631–49637
37. Mahammad, S., and Parmryd, I. (2015) Cholesterol depletion using methyl-β-cyclodextrin. *Methods Mol Biol*. **1232**, 91–102
38. Morenilla-Palao, C., Pertusa, M., Meseguer, V., Cabedo, H., and Viana, F. (2009) Lipid raft segregation modulates TRPM8 channel activity. *Journal of Biological Chemistry*. **284**, 9215–9224
39. Veliz, L. A., Toro, C. A., Vivar, J. P., Arias, L. A., Villegas, J., Castro, M. A., and Brauchi, S. (2010) Near-Membrane Dynamics and Capture of TRPM8 Channels within Transient Confinement Domains. *PLoS One*. **5**, e13290
40. Hilton, J. K., Rath, P., Helsell, C. V. M., Beckstein, O., and Van Horn, W. D. (2015) Understanding thermosensitive transient receptor potential channels as versatile polymodal cellular sensors. *Biochemistry*. **54**, 2401–2413
41. Garami, A., Shimansky, Y. P., Rumbus, Z., Vizin, R. C. L., Farkas, N., Hegyi, J., Szakacs, Z., Solymar, M., Csenkey, A., Chiche, D. A., Kapil, R., Kyle, D. J., Van Horn, W. D., Hegyi, P., and Romanovsky, A. A. (2020) Hyperthermia induced by transient receptor potential vanilloid-1 (TRPV1) antagonists in human clinical trials: Insights from mathematical modeling and meta-analysis. *Pharmacol Ther*. **208**, 107474
42. Ruzzi, F., Cappello, C., Semprini, M. S., Scalambra, L., Angelicola, S., Pittino, O. M., Landuzzi, L., Palladini, A., Nanni, P., and Lollini, P. L. (2024) Lipid rafts, caveolae, and epidermal growth factor receptor family: friends or foes? *Cell Commun Signal*. **22**, 489
43. Jakubík, J., and El-Fakahany, E. E. (2021) Allosteric Modulation of GPCRs of Class A by Cholesterol. *International Journal of Molecular Sciences 2021, Vol. 22, Page 1953*. **22**, 1953

44. Ballweg, S., Sezgin, E., Doktorova, M., Covino, R., Reinhard, J., Wunnicke, D., Hänelt, I., Levental, I., Hummer, G., and Ernst, R. (2020) Regulation of lipid saturation without sensing membrane fluidity. *Nature Communications 2020 11:1*. **11**, 1–13
45. Levental, I., Levental, K. R., and Heberle, F. A. (2020) Lipid Rafts: Controversies Resolved, Mysteries Remain. *Trends Cell Biol*. **30**, 341–353
46. Ernst, R., Ejsing, C. S., and Antonny, B. (2016) Homeoviscous Adaptation and the Regulation of Membrane Lipids. *J Mol Biol*. **428**, 4776–4791
47. Renne, M. F., and Ernst, R. (2023) Membrane homeostasis beyond fluidity: control of membrane compressibility. *Trends Biochem Sci*. **48**, 963–977
48. Hazel, J. R. (1995) THERMAL ADAPTATION IN BIOLOGICAL MEMBRANES: Is Homeoviscous Adaptation the Explanation? *AmlU. Rev. Physiol*. **57**, 19–42
49. Veatch, S. L., Cicuta, P., Sengupta, P., Honerkamp-Smith, A., Holowka, D., and Baird, B. (2008) Critical fluctuations in plasma membrane vesicles. *ACS Chem Biol*. **3**, 287–293
50. Zhang, X. D. (2010) Strictly Standardized Mean Difference, Standardized Mean Difference and Classical t-test for the Comparison of Two Groups. *Stat Biopharm Res*. **2**, 292–299
51. Zhang, X. D., Ferrer, M., Espeseth, A. S., Marine, S. D., Stec, E. M., Crackower, M. A., Holder, D. J., Heyse, J. F., and Strulovici, B. (2007) The Use of Strictly Standardized Mean Difference for Hit Selection in Primary RNA Interference High-Throughput Screening Experiments. *http://dx.doi.org/10.1177/1087057107300646*. **12**, 497–509
52. Dharan, R., Goren, S., Cheppali, S. K., Shendrik, P., Brand, G., Vaknin, A., Yu, L., Kozlov, M. M., and Sorkin, R. (2022) Transmembrane proteins tetraspanin 4 and CD9 sense membrane curvature. *Proc Natl Acad Sci U S A*. **119**, e2208993119
53. Schindelin, J., Arganda-Carreras, I., Frise, E., Kaynig, V., Longair, M., Pietzsch, T., Preibisch, S., Rueden, C., Saalfeld, S., Schmid, B., Tinevez, J. Y., White, D. J., Hartenstein, V., Eliceiri, K., Tomancak, P., and Cardona, A. (2012) Fiji: an open-source platform for biological-image analysis. *Nature Methods 2012 9:7*. **9**, 676–682
54. Luu, D. D., Ramesh, N., Can Kazan, I., Shah, K. H., Lahiri, G., Mana, M. D., Banu Ozkan, S., and Van Horn, W. D. (2024) Evidence that the cold- and menthol-sensing functions of the human TRPM8 channel evolved separately. *Sci Adv*. **10**, 9228
55. Strober, W. (1997) Trypan Blue Exclusion Test of Cell Viability. *Curr Protoc Immunol*. **21**, A.3B.1-A.3B.2

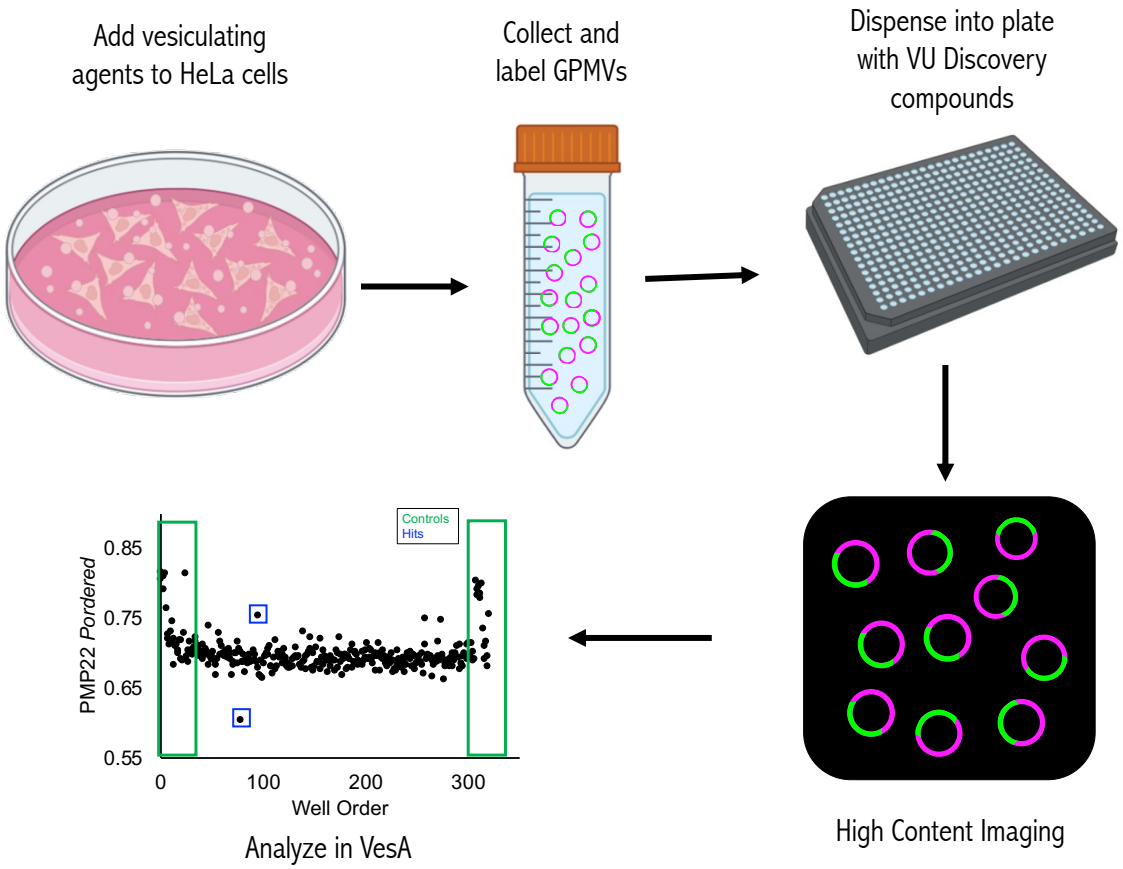

Figure 1. High-throughput screening identified modulators of PMP22 raft affinity. Pipeline used to screen 20,000+ compounds that identified hits described here.

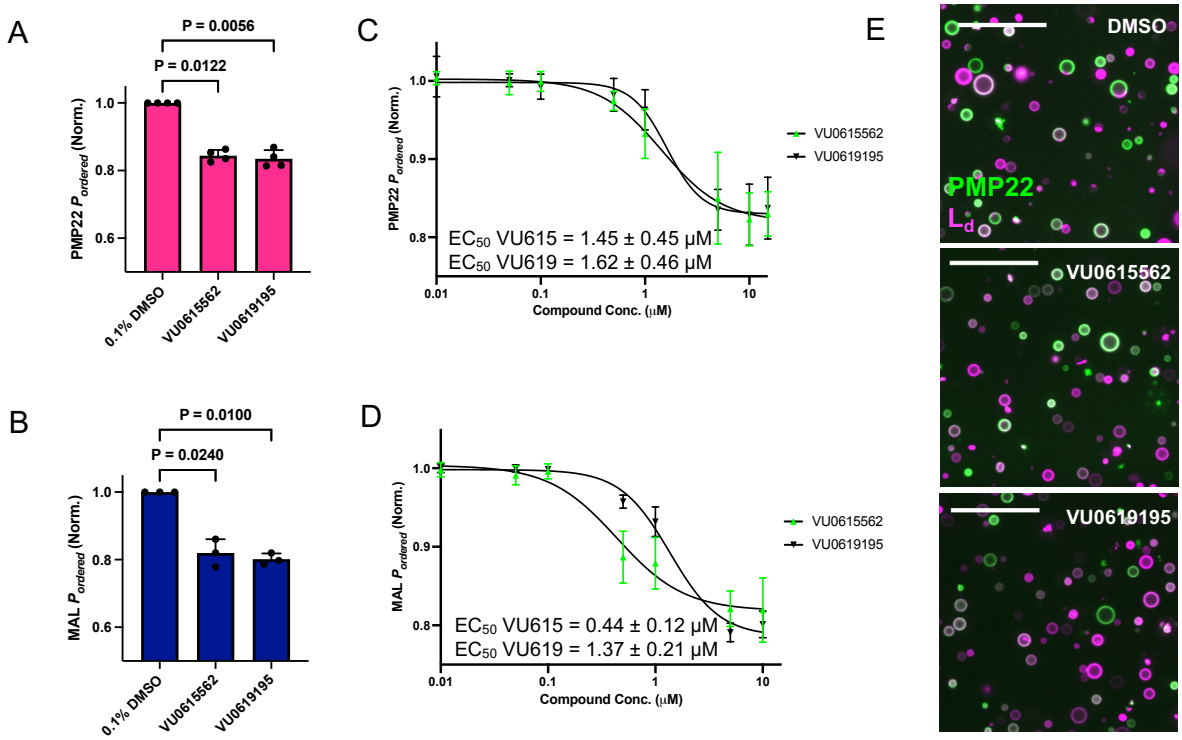

Figure 2. Modulators also affect PMP22 and MAL. A) Hit compounds VU0615562 and VU0619195 decrease ordered partitioning of PMP22 (n = 4) and B) MAL (n = 3) at 10 μM, Bars are means ± SD. P-values are from Mann-Whitney tests. C) Dose-response experiments determined EC50 for the impact of VU0615562 and VU0619195 on PMP22 ordered partitioning and D) MAL ordered partitioning. Points are mean ± SD, n = 3. Curves and EC50 values are from non-linear, sigmoidal fits, ± SE. E) Representative images of GPMVs treated with 10 μM compound. Scale bars are 50 μm.

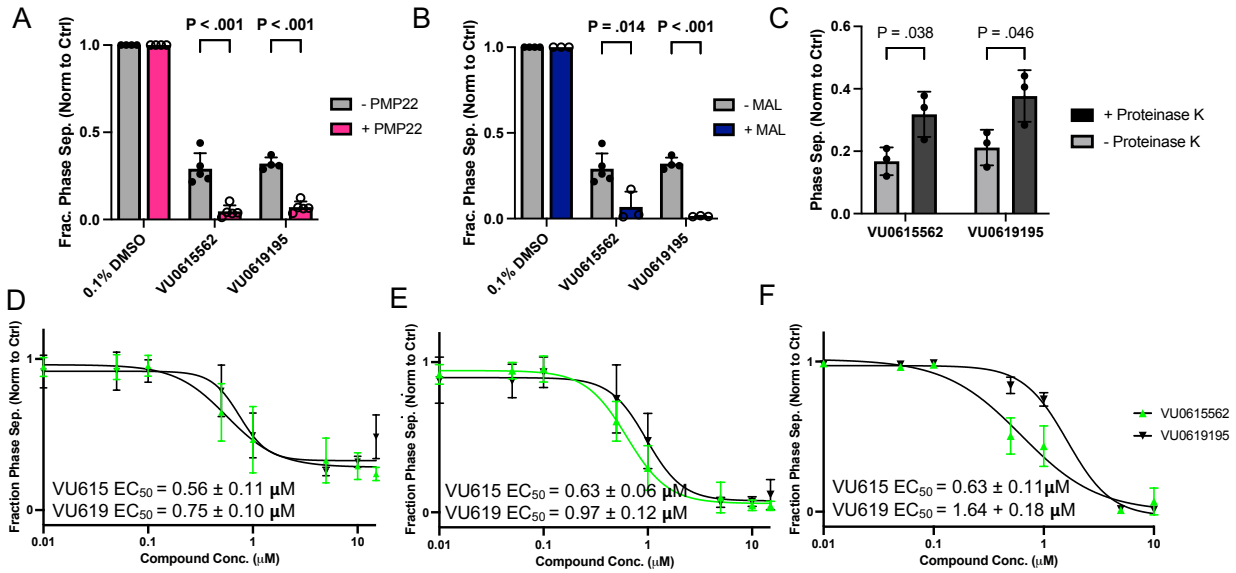

Figure 3. Compounds decrease phase-separation in a protein-dependent manner. A) Effects of VU0615562 and VU0619195 on the fraction of phase separated GPMVs with PMP22 (magenta bars) or from untransfected cells (gray bars) at 10 μM (*n* = 4-5). B) Effects of VU0615562 and VU0619195 on the fraction of phase separated GPMVs with MAL (navy bars) or from untransfected cells (gray bars) expression 10 μM (*n* = 3-5). C) Effects of compounds at 10 μM on the fraction of phase separated GPMVs with (dark gray bars) and without proteinase K treatment from untransfected cells (*n* = 3). Bars are means ± SD. P-values are from unpaired student's t-tests**. The bottom three panels present dose response experiments** determine EC50 values of compounds on phase separation in GPMVs from D) cells not expressing PMP22 or MAL, E) cells expressing PMP22, and F) cells expressing MAL. *n* = 3, points are means ± SD. Curves and EC50 values are from non-linear, sigmoidal fits.

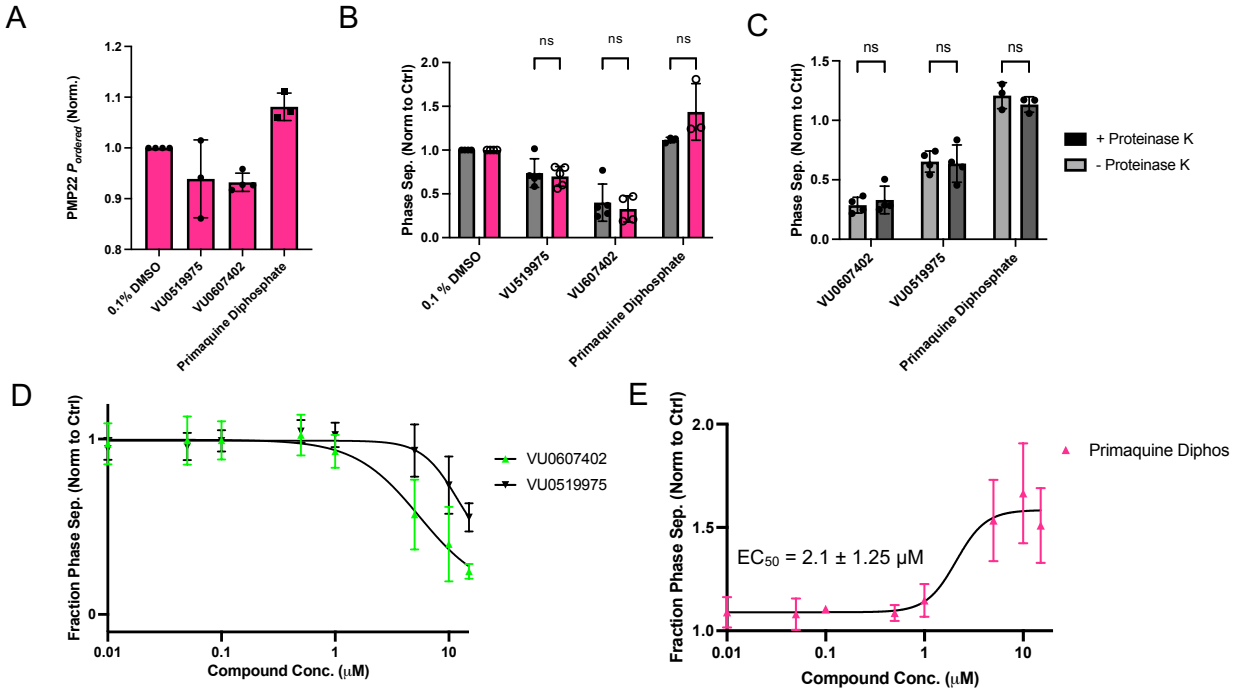

Figure 4. Screening identified raft modulators that are protein-independent. A) Effects of VU0519975, VU06107402, and primaquine diphosphate on ordered partitioning of PMP22 at 10 μM. Bars are means ± SD (*n* = 3) B) Effects of VU0519975, VU06107402, and primaquine diphosphate on phase separation with in GPMVs with PMP22 (magenta bars) or from untransfected cells (gray bars) PMP22 expression at 10 μM. Bars are means ± SD (*n* = 3-5) C) Effects of VU0519975, VU06107402, and primaquine diphosphate at 10 μM on GPMV phase separation with (dark gray bars) and without (gray bars) Proteinase K treatment from untransfected cells (*n* = 3-5). D) Dose response experiments with VU0519975 and VU06107402 (*n* = 3). E) Dose response experiments with primaquine diphosphate on phase separation. Points are means ± SD (*n* = 3). Curve and EC50 value from non-linear, sigmoidal fits ± SE.

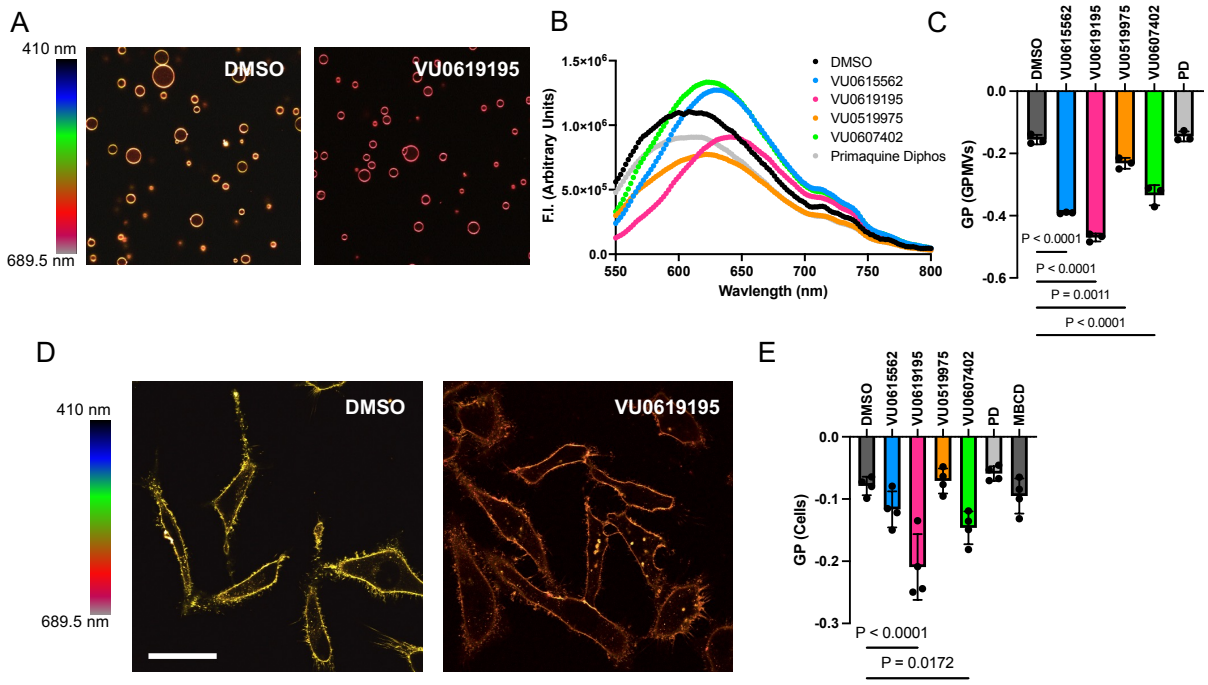

Figure 5. Compounds alter membrane fluidity in GPMVs and live cells. A) Representative spectral images (cropped from 40X fields) of GPMVs stained with Di-4 and treated with DMSO or VU0619195. B) Representative Di-4 emission spectra of GPMVs treated with 10 μM hit compounds. C) Generalized polarization values calculated from Di-4 emission spectra shown in B. Bars are means ± SD (*n* = 3). P-values are from ANOVA followed by Dunnett's multiple comparisons tests. D) Representative spectral images of live HeLa cells stained with Di-4 and treated with DMSO or VU0619195. Scale bar = 50 μm. E) Generalized polarization values calculated from Di-4 emission intensities calculated from individual cells as shown in D. Bars are means ± SD, 10-15 cells (technical replicates) per treatment were measured for each of 4 biological replicates. P-values are from ANOVA followed by Dunnett's multiple comparisons tests.

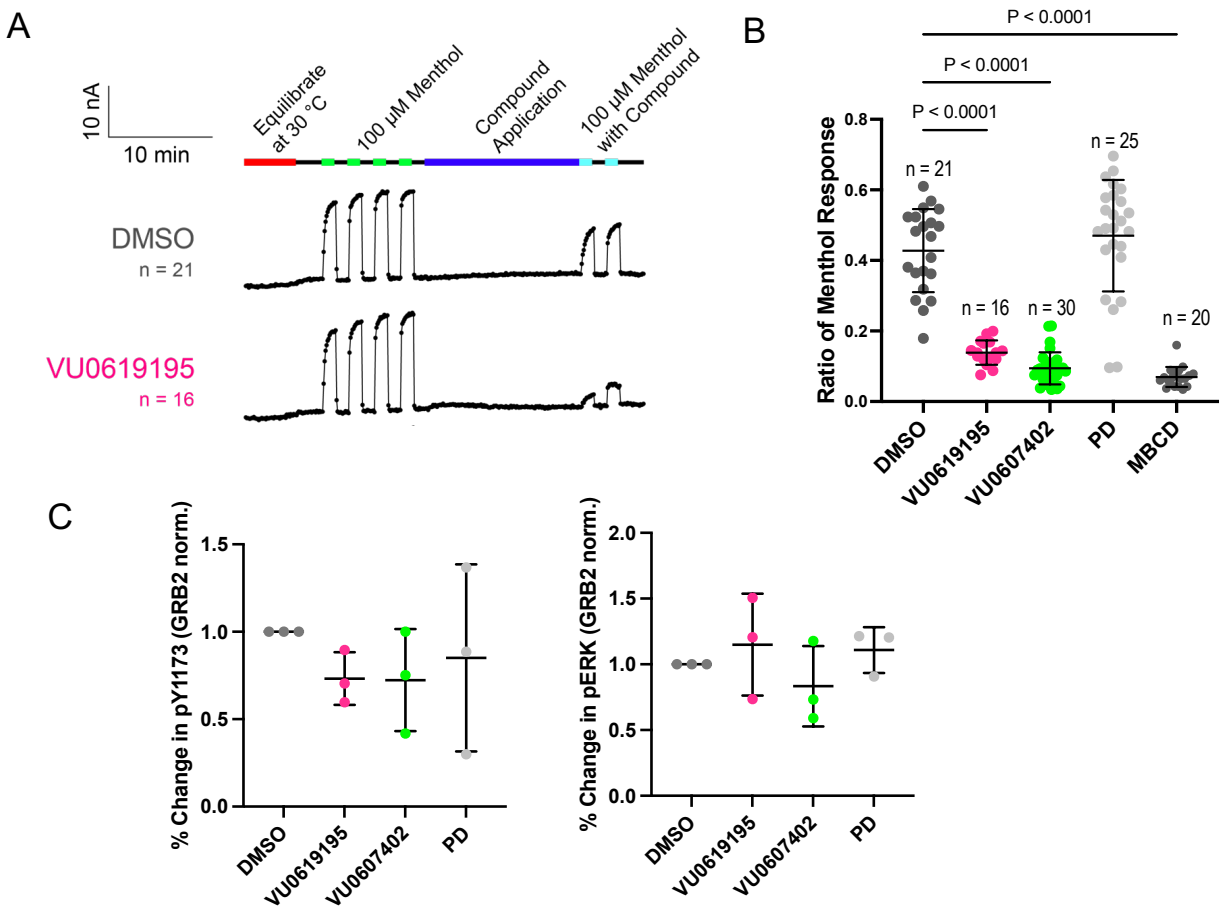

Figure 6. Compounds alter activity of TRPM8 but not EGFR. A) The average current traces of TRPM8 menthol response before and after exposure to the compounds in stably expressing full-length human TRPM8 HEK293T cells. Each dot is when the pulse program is applied. No perfusion was done in the first 5 minutes of the experiment to allow the automated patch clamp plate to equilibrate to 30 °C. Menthol was applied at 100 µM for 75 seconds 4 times to allow the menthol response to saturate before applying either 0.03% DMSO (control), 10 µM VU0619195, (See Supp. Fig. 8A for VU0607402, PD and MBCD). 0.03% DMSO concentration was kept consistent throughout the experiment. Menthol was then applied at 100 µM with the corresponding compounds twice for 75 seconds. Each n refers to the single sum of 20 cells from an amplifier on the automated patch clamp ensemble plate. B) The average ratio of menthol response from each compound in TRPM8 HEK293T cells. The ratio of menthol response uses the data from panel A and (Supp. Fig 8A), where the last two menthol response before compound application were averaged and compared to the two menthol response after compound application. Each n refers to the single sum of 20 cells from an amplifier on the automated patch clamp ensemble plate and are jittered. P-values were determined by ANOVA followed by Dunnett's tests. Bars are means ± SD. C) Results of Western blot analysis of phospho EGFR (left) and ERK (right) from HeLa cells treated with compounds for 15 min then stimulated with EGF for 1 min. n =3, bars are means ± SD. All comparisons are not significant.

Table 1. Protein-dependent compound structures and parameters

VU#	Structure	cLogP	FSP3	TPSA
VU0615562	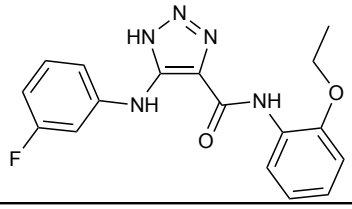	3.93	0.12	91.93
VU0619195	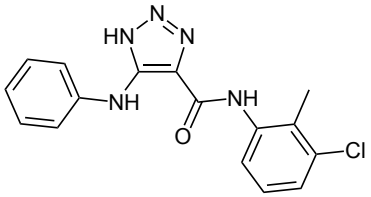	4.49	0.06	82.7

Table 2. Protein-independent compound structures and parameters

VU#	Structure	cLogP	FSP3	TPSA
VU0519975	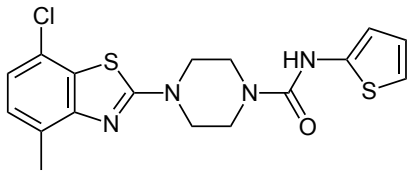	4.4	0.29	104.95
VU0607402	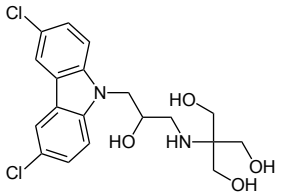	4.39	0.37	97.88
Primaquine Diphosphate	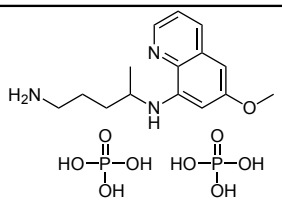	2.2	0.38	60.2